Charged-$K^*(890)$ production at 13 GeV/c

P. Estabrooks*
McGill University, Montreal, Canada

R. K. Carnegie
Carleton University, Ottawa, Canada

G. W. Brandenburgh,† R. J. Cashmore,‡ M. Davier,§ W. M. Dunwoodie, T. A. Lasinski, D. W. G. S. Leith, J. A. J. Matthews,¶ and P. Walden
Stanford Linear Accelerator Center, Stanford University, Stanford, California 94305
(Recieved 16 September 1977)

We present high-statistics data on differential cross sections and density matrix elements for $K^{*\pm}(890)$ production obtained in a 13-GeV/c SLAC experiment. The most remarkable features of the data are the dominance of natural-parity exchange and significant differences between K^{*+} and K^{*-} production by natural-parity isoscalar exchange. We present two exchange models which successfully describe this difference, as well as the overall t dependence: model A including Pomeron plus strongly exchange-degenerate Regge poles and model B involving broken exchange degeneracy for the f and ω exchanges. These two phenomenological models lead to different predictions for the energy dependence of $K^{*\pm}$ production, for the relative $K^*(1420)/K^*(890)$ production rate, and for the SU(3)-related $\rho^{\pm}$ production processes.

I. INTRODUCTION

In a spectrometer experiment at SLAC, we have obtained data on the reactions

$$K^-p \to K^{*-}(890)p\ , \tag{1}$$

$$K^+p \to K^{*+}(890)p \tag{2}$$

at 13 GeV/c. These reactions can proceed via the positive, and negative-G-parity, isoscalar and isovector t-channel exchanges as shown in Table I. Fortunately, the nature of the isovector exchanges is known[1,2] from studies of the charge exchange reactions

$$K^-p \to \overline{K}^{*0}(890)n\ , \tag{3}$$

$$K^+n \to K^{*0}(890)p\ , \tag{4}$$

at 4 and 13 GeV/c (Refs. 3 and 4). Data for the ρ production reactions analogous to reactions (1)–(3) are sufficient to isolate the t-channel isoscalar exchanges[5,6] in a model-independent way. Here, however, the coexistence of both positive- and negative-G-parity exchanges means that model-independent isolation of isoscalar exchange would require data for charged-K^* production on neutrons. Since no data of sufficiently high statistics exist, such a separation must invoke some model-dependent assumptions.

In Sec. II we discuss the experimental data and present differential cross sections and density matrix elements for reactions (1) and (2). In Sec. III, we discuss the features of these data, particularly in comparison with reaction (3). This leads, in Sec. IV, to model fits to the data for all three reactions. We find that either (A) a model involving exchange-degenerate (EXD) f-ω Regge poles and a small [SU(3)-forbidden] Pomeron coupling to KK^*, or (B) a model with ω and f trajectories which are not exchange degenerate, provides a good description of the data. In Sec. V we present the predictions of both models for charged-$K^*(1420)$ production, for the energy dependence of charged-$K^*(890)$ production, as well as the SU(3) comparison with the isoscalar-exchange contribution to ρ production. We discuss the constraints that these other data place on any Regge-type model of the $I_t = 0$ contributions to K^* production.

TABLE I. Contributions of different t-channel isospin and G-parity exchanges to the amplitudes for K^* production.

	$I=1$		$I=0$	
	$G=-1(A_2)$	$G=+1(\rho)$	$G=+1(f)$	$G=-1(\omega)$
$K^-p \to K^{*-}p$	$\frac{1}{2}$	$-\frac{1}{2}$	$\frac{1}{2}$	$-\frac{1}{2}$
$K^+p \to K^{*+}p$	$\frac{1}{2}$	$\frac{1}{2}$	$\frac{1}{2}$	$\frac{1}{2}$
$K^-p \to \overline{K}^{*0}n$	1	−1	0	0
$K^-n \to K^{*-}n$	$-\frac{1}{2}$	$\frac{1}{2}$	$\frac{1}{2}$	$-\frac{1}{2}$
$K^+n \to K^{*+}n$	$-\frac{1}{2}$	$-\frac{1}{2}$	$\frac{1}{2}$	$\frac{1}{2}$
$K^+n \to K^{*0}p$	1	1	0	0

II. EXPERIMENTAL RESULTS

An experiment studying several topics in K^*-meson spectroscopy and production dynamics has been performed at SLAC using 13-GeV/c rf-separated $K^\pm$ beams incident on a 1-m liquid hydrogen target. A plan view of the apparatus is shown in Fig. 1. Events originating in the hydrogen target with two or more forward charged particles passing through the 18-kgm dipole analyzing magnet were selected by the trigger system. The wire chamber spectrometer system was used to detect, measure, and identify these forward charged particles as well as the incident kaon. The charged-$K^*(890)$ production reactions (1) and (2) can therefore be studied using events corresponding to the decay chain

$$K^*(890) \to K^0\pi^\pm,$$

with

$$K^0 \to \pi^+\pi^-,$$

which provides an all charged-particle final state. In order to minimize the K^+/K^- relative normalization uncertainty associated with possible changes in apparatus performance, several periods of K^+ and K^- data collection were interleaved. In addition, very large samples of $K^\pm \to \pi^\pm\pi^+\pi^-$ beam decays (also a 3π final state) were obtained at the same time as the K^* data and provided a direct measurement of the uncertainty in the K^+/K^- relative normalization; this was found to be $\pm 2\%$.

The forward part of the spectrometer, which measured the momenta and trajectories of all three pions from the $(K^0\pi)^\pm$ system, included three scintillation-counter hodoscopes and nine magnetostrictive-readout wire spark chambers, four upstream and five downstream of the dipole magnet. Each spark chamber consisted of two gaps with four readout planes and was deadened in the beam region with small polyurethane plugs. The dipole aperture was 0.6 m by 1.8 m. Events containing a forward K^0 were selected in the reconstruction program by first calculating the $\pi^+\pi^-$ invariant mass for each charge zero pairing of

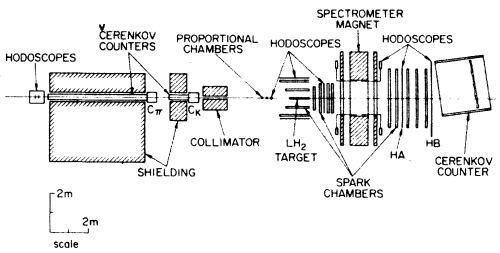

FIG. 1. Plan view of the experimental apparatus.

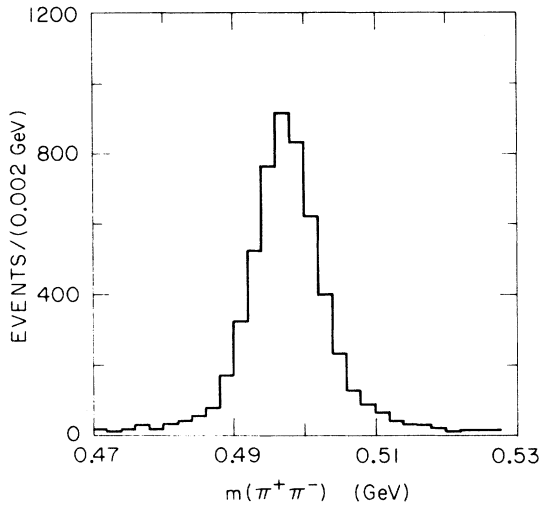

FIG. 2. Observed $\overline{K}^0 \to \pi^+\pi^-$ mass distribution for events from the reaction $K^-p \to \overline{K}^0\pi^-p$ with $0.84 < m(\overline{K}^0\pi^-) < 0.94$ GeV.

tracks. Then, for candidates within 30 MeV of the K^0 mass, that pair of tracks was required to form a good vertex within a decay region including the hydrogen target volume and extending downstream to just before the second spark chamber. The reconstructed K^0 trajectory was then used with the third forward pion and the incident kaon to determine the primary vertex. The secondary K^0 vertex was required to be at least 3.8 cm downstream of the primary vertex. The $\pi^+\pi^-$ invariant mass distribution for events otherwise satisfying the criteria for reaction (1) is shown in Fig. 2. The K^0 mass resolution is 10.5 MeV full width at half maximum (FWHM). In addition to the vertex cuts, we also required that the $\pi^+\pi^-$ invariant mass be in the mass interval $0.488 < m(\pi^+\pi^-) < 0.508$ GeV to define our $K^0\pi$ data sample.

Events with a recoil proton are selected by requiring that the missing mass (MM) recoiling against the $(K^0\pi)^\pm$ system lie in the range $0.70 < \mathrm{MM} < 1.05$ GeV. The observed MM distributions for the $(K^0\pi)^\pm$ system in the $K^*(890)$ region, $0.84 < m(K^0\pi^\pm) < 0.94$ GeV, are shown in Figs. 3(c) and 3(d) for the K^+ and K^- data, respectively. The prominent proton peak has an FWHM = 165 MeV and is well separated from the recoil-Δ^+ events and higher missing-mass continuum. If we now select recoil-proton events using the MM cut, we obtain the observed $K^0\pi^\pm$ invariant mass distributions shown in Figs. 3(a) and 3(b). The $K^*(890)$ accounts for most of the events. In order to display the small $K^*(1420)$ peak, the vertical scale has been changed in the vicinity of the $K^*(890)$ peak. The final $K^{*\pm}(890)p$ data sample, defined as

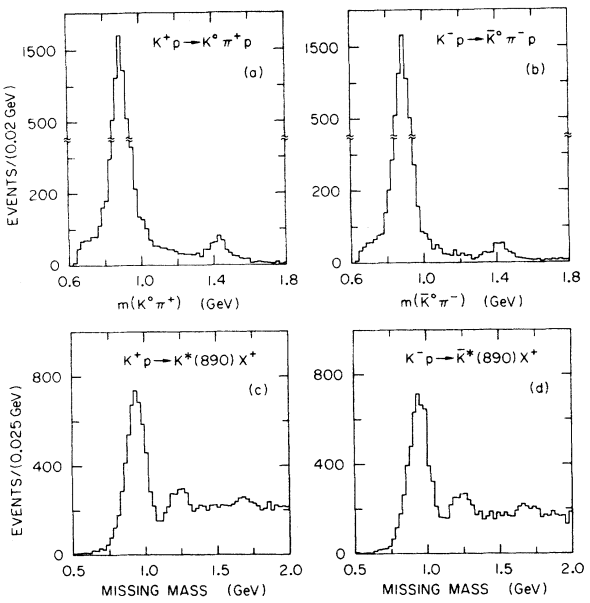

FIG. 3. (a), (b) Observed $K^0\pi$ mass distributions for the reactions $Kp \to (K^0\pi)p$. (c), (d) Observed missing-mass distributions for $K^{\pm}p \to (K^0\pi)^{\pm}X^+$ with $0.84 < m(K^0\pi) < 0.94$ GeV.

events with $0.84 < m(K^0\pi^{\pm}) < 0.94$ GeV, contains 5136 $K^{*+}(890)$ events and 4911 $\overline{K}^{*-}(890)$ events.

The $K^{\pm}p \to (K^0\pi)^{\pm}p$ differential cross section and the t-channel spherical harmonic moments, $\langle Y_{LM} \rangle$, of the $K^0\pi$ decay angular distribution have been measured as a function of momentum transfer for the $K\pi$ mass interval $0.84 < m(K^0\pi) < 0.94$ GeV. The cross sections and moments were obtained using a maximum-likelihood fitting procedure to correct the observed $K\pi$ data for the effects of the spectrometer acceptance. The spectrometer acceptance was determined using a Monte Carlo program which included the effects of geometric acceptance, decay and absorption of secondary particles, apparatus efficiency, resolution, and imposed $K^0\pi$ topological and kinematic cuts that were identical to those applied to the data. In the $K^*(890)$ region, the average acceptance of the spectrometer for the $K^0\pi^{\pm}$ final states is ~15%, as determined by the ratio of the number of observed events to the number of events found from the likelihood fits; it varied slowly as a function of momentum transfer. This result includes all of the geometrical, decay, and absorption factors mentioned above; it does not include the $K^0 \to \pi^+\pi^-$ branching ratio. The corresponding acceptance for events in the $K^*(1420)$ region is ~0.03. In the fits to the $K\pi$ angular distributions, only moments with L, $M \leq 2$ have been included, since only S and P waves are present.

The $K^{\pm} \to (K^0\pi)^{\pm}p$ differential cross sections, $d\sigma/dt$, for this $K^0\pi$ mass interval, corrected for the $K^0 \to \pi^+\pi^-$ decay branching ratio, are given in Table II and shown in Fig. 4 for $-t < 1.0$ GeV^2. While the cross sections for the K^+- and K^--initiated reactions are equal near $t = 0$, the K^- cross section is 25% larger than the K^+ at $t = 0.1$ GeV^2. In contrast, the K^+ cross section is much larger than the K^- at large momentum transfer. The K^+/K^- crossover occurs near $t \sim 0.3$ GeV^2. Recall that the uncertainty in the relative K^+/K^- normalization is $\pm 2\%$.

The $K\pi$ angular distribution results, expressed as elements of the t-channel spin density matrix, $\rho^{LL'}_{MM'}$, are presented in Table II and Fig. 5. The striking overall feature is the very similar behavior of the K^+ and K^- density matrix elements despite the cross-section differences. The values of $(\rho^{11}_{00} - \rho^{11}_{11})$ and ρ^{11}_{1-1} indicate that natural-parity exchange dominates $K^{*\pm}(890)$ production except near $t = 0$. Although the interference density matrix elements are small, they remain nonzero for all t values indicating both a small S-wave contribution to the $K^0\pi$ cross section and the existence of an unnatural-parity-exchange contribution over the full momentum-transfer range. The particular linear combinations of density matrix elements

$$\sigma_0 = (\rho^{11}_{00} + \rho^{00}_{00}/3)d\sigma/dt,$$
$$\sigma_{\pm} = (\rho^{11}_{11} \pm \rho^{11}_{1-1} + \rho^{00}_{00}/3)d\sigma/dt, \quad (5)$$

project out helicity-zero $K^*(890)$ production via unnatural-parity exchange (σ_0), and to a good approximation at 13 GeV/c, helocity-one $K^*(890)$ production via natural- (σ_+) and unnatural- (σ_-)

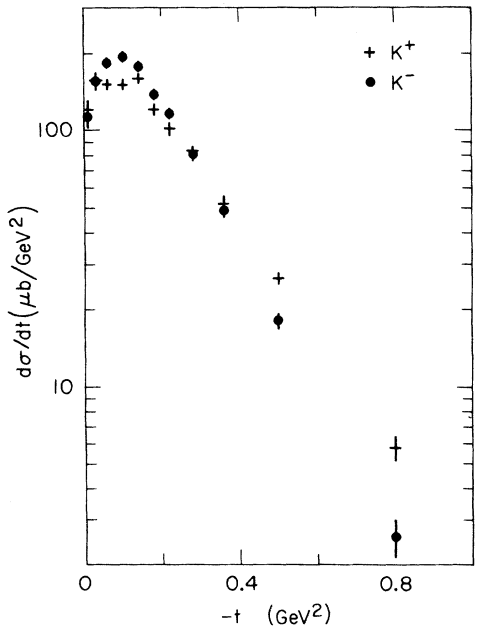

FIG. 4. Differential cross sections for $K^{\pm}p \to (K^0\pi)^{\pm}p$ with $0.89 < m(K^0\pi) < 0.94$ GeV.

TABLE II. Differential cross section and $K^0\pi$ density matrix elements in the t channel.

t (GeV^2)	$d\sigma/dt$ (μb/GeV^2)	$\rho^{11}_{00}-\rho^{11}_{11}$	ρ^{11}_{1-1}	Reρ^{11}_{10}	Reρ^{10}_{00}	Reρ^{10}_{10}
		(a) $K^+p\to(K^0\pi^+)p$ $0.84<m(K^0\pi^+)<0.94$ GeV				
0.00–0.02	121.0 ± 9.8	0.183 ± 0.086	0.162 ± 0.030	−0.060 ± 0.026	0.112 ± 0.038	−0.021 ± 0.015
0.02–0.04	156.6 ± 11.2	0.047 ± 0.079	0.251 ± 0.031	−0.044 ± 0.023	0.091 ± 0.033	0.001 ± 0.013
0.04–0.08	151.0 ± 6.7	−0.262 ± 0.049	0.373 ± 0.022	−0.032 ± 0.015	0.025 ± 0.020	0.002 ± 0.010
0.08–0.12	150.7 ± 6.7	−0.331 ± 0.047	0.361 ± 0.025	−0.030 ± 0.016	0.035 ± 0.019	−0.008 ± 0.012
0.12–0.16	159.7 ± 7.2	−0.288 ± 0.043	0.381 ± 0.024	−0.049 ± 0.017	0.022 ± 0.018	−0.013 ± 0.009
0.16–0.20	121.1 ± 6.1	−0.338 ± 0.055	0.446 ± 0.028	−0.023 ± 0.019	0.025 ± 0.020	−0.003 ± 0.012
0.20–0.24	101.3 ± 6.2	−0.414 ± 0.045	0.471 ± 0.051	−0.025 ± 0.026	−0.012 ± 0.023	0.053 ± 0.019
0.24–0.32	83.3 ± 3.7	−0.433 ± 0.037	0.371 ± 0.025	−0.025 ± 0.015	0.030 ± 0.016	−0.026 ± 0.013
0.32–0.40	52.1 ± 3.5	−0.352 ± 0.050	0.451 ± 0.060	−0.083 ± 0.022	−0.033 ± 0.024	−0.034 ± 0.024
0.40–0.60	26.6 ± 1.5	−0.478 ± 0.044	0.492 ± 0.036	−0.017 ± 0.018	0.008 ± 0.017	−0.020 ± 0.016
0.60–1.00	5.8 ± 0.6	−0.300 ± 0.101	0.433 ± 0.083	−0.036 ± 0.030	−0.052 ± 0.032	0.066 ± 0.036
		(b) $K^-p\to(K^0\pi^-)p$ $0.84<m(K^0\pi^-)<0.94$ GeV				
0.00–0.02	113.1 ± 10.5	0.161 ± 0.093	0.164 ± 0.035	−0.103 ± 0.028	0.107 ± 0.042	−0.032 ± 0.016
0.02–0.04	154.8 ± 10.8	−0.192 ± 0.079	0.360 ± 0.034	−0.011 ± 0.027	0.036 ± 0.035	−0.016 ± 0.013
0.04–0.08	184.2 ± 7.8	−0.365 ± 0.050	0.424 ± 0.020	−0.039 ± 0.013	0.028 ± 0.018	−0.004 ± 0.007
0.08–0.12	193.3 ± 8.3	−0.293 ± 0.051	0.392 ± 0.024	−0.042 ± 0.013	0.033 ± 0.020	−0.013 ± 0.011
0.12–0.16	178.4 ± 7.7	−0.309 ± 0.045	0.428 ± 0.021	−0.041 ± 0.013	0.035 ± 0.018	−0.014 ± 0.010
0.16–0.20	137.9 ± 7.5	−0.420 ± 0.053	0.473 ± 0.039	−0.009 ± 0.021	−0.035 ± 0.022	0.018 ± 0.018
0.20–0.24	117.0 ± 6.2	−0.409 ± 0.049	0.431 ± 0.029	−0.022 ± 0.018	0.023 ± 0.023	−0.017 ± 0.015
0.24–0.32	80.6 ± 4.7	−0.448 ± 0.039	0.482 ± 0.053	0.001 ± 0.024	0.023 ± 0.019	−0.027 ± 0.018
0.32–0.40	48.8 ± 3.0	−0.462 ± 0.061	0.487 ± 0.042	−0.005 ± 0.013	0.010 ± 0.018	−0.010 ± 0.016
0.40–0.60	18.0 ± 1.3	−0.352 ± 0.063	0.437 ± 0.034	−0.029 ± 0.019	−0.054 ± 0.030	0.030 ± 0.020
0.60–1.00	2.6 ± 0.4	−0.221 ± 0.147	0.407 ± 0.213	0.029 ± 0.078	0.002 ± 0.068	0.018 ± 0.071

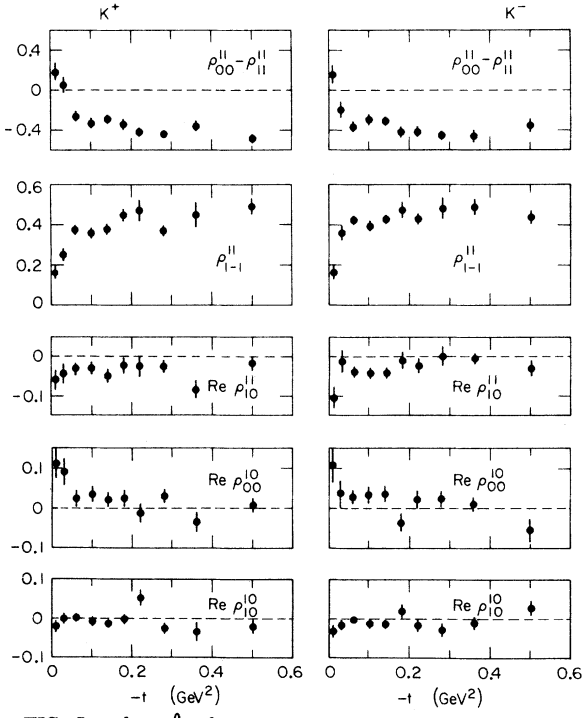

FIG. 5. The $K^0\pi$ density matrix elements in the t-channel helicity frame for the reactions $K^\pm p\to(K^0\pi)^\pm p$ with $0.84<m(K^0\pi)<0.94$ GeV.

parity exchange. In addition, each of these partial cross sections contains a small S-wave $K\pi$ contribution through the term $\frac{1}{3}\rho^{00}_{00}\,d\sigma/dt$. The decomposition of the $K^\pm p\to(K^0\pi)^\pm p$ differential cross sections into the two largest contributions σ_+ and σ_0 is shown in Fig. 6(a) for the K^+ and K^- reactions. This plot demonstrates quite clearly the dominance of the natural-parity-exchange contribution to $K^*(890)$ production.

In order to determine the $K^\pm p\to K^{*\pm}(890)p$ cross sections we must (i) correct for the small S-wave contribution to the cross section, (ii) account for the portion of the $K^*(890)$ Breit-Wigner line shape which lies outside our mass interval, and (iii) correct for the unseed $K^{*\pm}(890)\to K^\pm\pi^0$ decay mode with a Clebsch-Gordan factor. The S-wave contribution to these data has been measured through studies of the analogous charge-exchange reaction $K^-p\to\bar{K}^*(890)n$ as discussed in Sec. IV of this paper and in Ref. 2. The S wave accounts for only 3% of the $K^0\pi$ cross section in this mass interval. We have multiplied our cross sections by 1.35 to account for that part of the P wave $K^*(890)$ Breit-Wigner line shape outside our $K^0\pi$ mass cut. The final integrated $K^\pm p\to K^{*\pm}(890)p$ cross sections for $0<t<1.0$ GeV^2 are 101 ± 2 μb for the K^+ reaction and 104 ± 2 μb for the K^- reaction

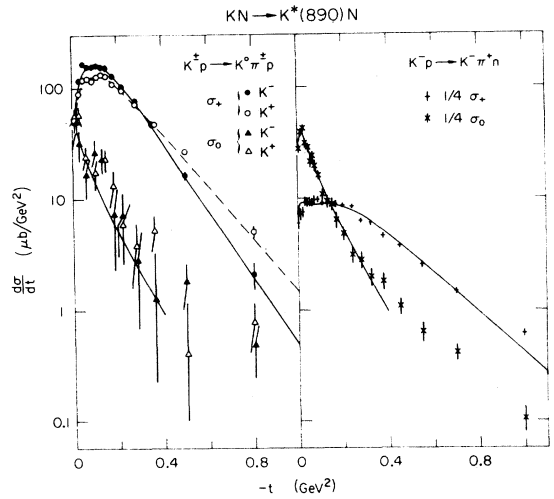

FIG. 6. The t-channel partial cross sections, σ_+ and σ_0, for the reactions $K^-p \to \bar{K}^0\pi^-p$, $K^+p \to K^0\pi^+p$, and $K^-p \to \bar{K}^{*0}n$ at 13 GeV/c. The K^* regions are defined by $0.84 < M(K^0\pi^\pm) < 0.94$ GeV and $0.87 < M(K^-\pi^+) < 0.92$ GeV. The factor of 4 in the $K^-\pi^+$ data plotted is included to equate the t-channel isovector contributions to the charge-exchange and noncharge-exchange cross sections. Moreover, the $K^-\pi^+$ data have been "renormalized" to correspond to a 100-MeV mass cut, assuming that the cross sections are described by P-wave Breit-Wigner resonance forms. The solid (dashed) curves, corresponding to the K^- (K^+) initiated reactions, result from fits involving cuts, Pomeron, and strongly exchange-degenerate Regge poles, as described in the text.

where the errors quoted are the statistical errors only. In addition, there is the relative normalization uncertainty of ± 2% and a common possible systematic error in absolute normalization of ± 10%. We see that the integrated K^+ and K^- cross sections are equal within errors despite the very different momentum-transfer dependence of the two reactions.

III. FEATURES OF THE $K^{*\pm}(890)$ PRODUCTION DATA

The most striking feature of the $K^\pm p \to K^0\pi^\pm p$ reactions is the dominance of natural-parity exchange. This has been shown in Fig. 6 where σ_+ and σ_0 for these non-charge-exchange reactions are presented. In addition, these cross sections are compared with $\sigma_+/4$ and $\sigma_0/4$ for the charge-exchange (CEX) reaction, corrected to correspond to the same $M_{K\pi}$ interval as the non-CEX reactions. From examination of Fig. 6, we also see that σ_0 is the same for the two non-CEX (NCEX) reactions and is equal to that for the CEX reaction, thus implying that only isovector exchanges contribute to the t-channel helicity-zero amplitudes. Moreover, the remaining four unnatural-parity-exchange cross sections (σ_-, σ_{10}, σ_{0s}, and σ_{1s}), although small and not very well determined, are also consistent with being equal in all three reactions. Therefore, we conclude that unnatural-parity isoscalar exchanges do not contribute significantly to $K^{*\pm}$ production.

On the other hand, σ_+ for $K^{*\pm}$ production is about ten times as large as that due to the isovector contribution alone. This is not surprising, since natural-parity isoscalar f and ω Regge exchanges, as well as possible Pomeron exchange, are expected to be important. In fact, the dominance of natural-parity exchange in $K^{*\pm}$ production has been observed[7] over a range of energies from 3 to 16 GeV/c, with the fraction of the cross section due to natural-parity exchange increasing with energy.

In this experiment using both K^+ and K^- incident beams, we find that not only does natural-parity exchange dominate $K^{*\pm}$ production, but that there are significant differences in σ_+ between the K^+- and K^--initiated reactions. For $0.02 \lesssim -t \lesssim 0.3$ GeV^2, the K^{*-} cross section is significantly larger than that for K^{*+} production, whereas for $|t| > 0.4$ GeV^2 the converse holds. These differences are much larger than the entire isovector-exchange cross section. Furthermore, isoscalar exchanges such as f, ω, P are known[8] to couple dominantly to nucleon nonflip amplitudes whereas isovector exchanges such as ρ, A_2 couple much more strongly to nucleon flip amplitudes, so that there should be little isovector-isoscalar interference. Thus we conclude that the K^+/K^- difference is a feature of the isoscalar exchanges.

The difference between K^{*+} and K^{*-} production must be due to interference between positive- and negative-G-parity exchanges (see, for instance, Table I). Possible natural-parity isoscalar exchanges are P, f, and ω. Note that if the Pomeron were a pure SU(3) singlet, it could not contribute to K^* production. The difference between πp and Kp cross sections at high energies is already an indication of a significant non-SU(3)-singlet component of the Pomeron. The difference between K^{*+} and K^{*-} production can be written as

$$\Delta_+ \equiv \sigma_+(K^{*+}) - \sigma_+(K^{*-})$$
$$= 4\,\mathrm{Re}(P+f)\omega^* . \qquad (6)$$

If f and ω are even weakly exchange degenerate, i.e., $\alpha_f = \alpha_\omega$, then Re $(f\omega^*) = 0$ and the only contribution to Δ_+ comes from P-ω interference. In Fig. 7(a) we show, for three different t values, P, ω (and f) contributions[9] to the nucleon nonflip amplitudes which can reproduce the K^{*+}, K^{*-} difference seen in the data of Fig. 6. From the relative signs of P and ω at small values of mo-

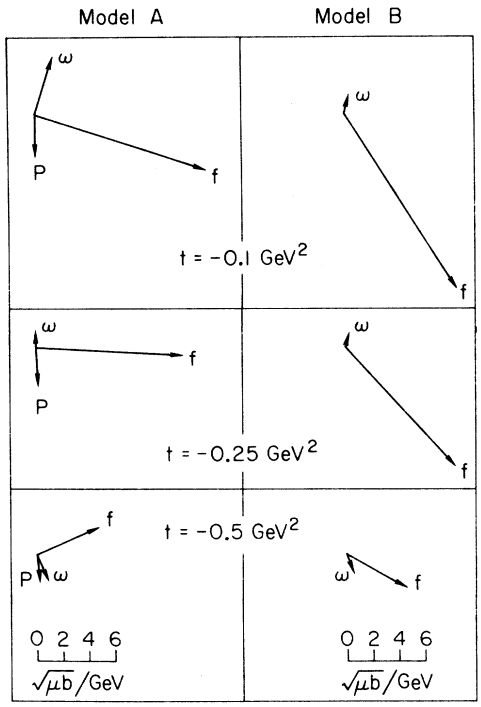

FIG. 7. The isoscalar contributions to the nucleon spin-nonflip, natural-parity-exchange amplitudes, P_+^n, for the reaction $K^+p \to K^{*0}(890)p$ at 13 GeV/c. Model A consists of Pomeron and strongly exchange-degenerate f-ω t-channel exchanges while model B has contributions from non-exchange-degenerate f and ω only. The values of the parameters specifying these exchanges were obtained from least-squares fits to the data of Table II, as described in the text.

mentum transfer and the fact that the Pomeron trajectory is significantly flatter than the ω trajectory, it is clear that the crossover in σ_+ at $-t \sim 0.4$ GeV^2 must be attributed to a zero in the ω (or, in principle, the P) exchange contribution rather than to complete phase incoherence of P and ω. Since the crossover occurs in the vicinity of an expected nonsense wrong-signature zero for the ω, it is reasonable to associate these two phenomena.

On the other hand, if there is no Pomeron contribution to K^* production, then the K^+/K^- difference must be due to f-ω interference. This requires ω-f exchange degeneracy to be broken, $\alpha_f \neq \alpha_\omega$. Historical precedent for such a picture is provided by the observed inequality of the ρ and A_2 trajectories as extracted from the energy dependence of the cross sections for charge-exchange pseudoscalar-meson production.[10] Since the f is expected[11] to have a higher and flatter trajectory than the ω and since the relative signs of the two contributions are determined [as shown in Fig. 7(b) and discussed in detail in Sec. IV] by the sign of Δ_+ at small momentum transfer,[12] it is again the case that the $-t \sim 0.4$ GeV^2 crossover in σ_+ is most readily explained as being due to the ω nonsense wrong-signature zero.

IV. THE MODELS

A. The parametrization

A complete description of reactions (1) and (2) requires not only the dominant natural-parity-exchange isoscalar contributions but also isovector and unnatural-parity contributions. As in Ref. 2, we can describe these data in terms of strongly exchange-degenerate (EXD) Regge poles and "cuts" which contribute only to t-channel K^* helicity-one, nucleon spin-flip amplitudes. The parametrization of the nucleon spin-flip (nonflip) amplitude $L^{f(n)}_{\lambda\pm}$ for spin L, t-channel helicity λ, K^* production by natural- (unnatural-) parity exchange is thus

$$
\begin{aligned}
&S_0^n = P_0^n = P_-^n = 0,\\
&P_0^f = \pi \pm B = G_{\pi B}\,\frac{\sqrt{-t}}{\mu^2 - t}\, e^{b_\pi t}\, \mathcal{S}^\pm_{\pi B}\,,\\
&S_0^f = \gamma_S e^{i\Delta_S} e^{b_S t} P_0^f\,,\\
&P_-^f = C = G_C\, e^{b_C t}\, \mathcal{S}^\pm_{\pi B}\,,\\
&P_+^f = C + A_2 \pm \rho = C + (-t) G_{A\rho} e^{b_A t} \mathcal{S}^\pm_{A\rho}\,,\\
&P_+^n(\mathrm{CEX}) = \frac{\sqrt{-t}}{4}\, G_{A\rho} e^{b_A t} \mathcal{S}^\pm_{A\rho}\,,
\end{aligned}
\tag{7}
$$

where the Regge-signature-factor combinations are given by

$$\mathcal{S}^\pm_{\pi B} = \tfrac{1}{2}(1 + e^{-i\pi\alpha_\pi}) \pm \tfrac{1}{2}(1 - e^{-i\pi\alpha_\pi})\,, \tag{8a}$$

$$\mathcal{S}^\pm_{A\rho} = \frac{\Gamma(1-\alpha_A)}{2}\left[(1 + e^{-i\pi\alpha}) \pm (1 - e^{-i\pi\alpha_A})\right]. \tag{8b}$$

Here the $\pm$ signs refer to the $K^\pm$-initiated reactions, and the subscripts 0, +, − refer to the t-channel helicity of the produced K^* and to the exchange naturality. The trajectories are given by

$$
\begin{aligned}
&\alpha_\pi = t - \mu^2\,,\\
&\alpha_A = \tfrac{1}{2} + t\,.
\end{aligned}
\tag{9}
$$

We use two different models to describe the (natural-parity) isoscalar exchanges, which we assume contribute only to the nucleon spin-nonflip amplitudes, P_+^n(NCEX). In model A, we parametrize P_+^n as

$$
\begin{aligned}
P_+^n(\mathrm{NCEX}) &= P + (f \pm \omega)_{\mathrm{EXD}}\\
&= \sqrt{-t}\,(G_P e^{b_P t}\, e^{i(\pi/2)\alpha_P} + G^{\mathrm{EXD}}_{f\omega}\, e^{b_{f\omega} t}\, \mathcal{S}^\pm_{f\omega})\,,
\end{aligned}
\tag{10a}
$$

with $\alpha_P = 1 + 0.2t$ and $\mathcal{S}^{\pm}_{f\omega}$ given by the exchange-degenerate form of $\alpha^{\rm EXD}_{f\omega}$ parametrized as

$$\alpha^{\rm EXD}_{f\omega}(t) = 1 + \alpha'_E(t - m_\omega^2) \ . \tag{11a}$$

Model B, with no Pomeron contribution, describes P^n_+ as

$$P^n_+({\rm NCEX}) = f \pm \omega = \sqrt{-t}\,(G_f \mathcal{S}_f e^{b_f t} \pm G_\omega \mathcal{S}_\omega e^{b_\omega t}) \ , \tag{10b}$$

where the Regge signature factors $\mathcal{S}_f$ and $\mathcal{S}_\omega$ are given by

$$\mathcal{S}_f = \tfrac{1}{2}\Gamma(1 - \alpha_f(t))\,(1 + e^{-i\pi\alpha_f(t)}) \ , \qquad \mathcal{S}_\omega = \tfrac{1}{2}\Gamma(1 - \alpha_\omega(t))\,(1 - e^{-i\pi\alpha_\omega(t)}) \ . \tag{12}$$

The effective f trajectory, α_f, is constrained to be a linear function of t and to pass through the f and h mesons, while α_ω is linear in t and constrained to go through the ω, that is,

$$\alpha_f = 0.72 + 0.79t, \quad \alpha_\omega = 1 + \alpha'_\omega(t - m_\omega^2) \ . \tag{11b}$$

The relation between the partial cross sections of Fig. 6 and the amplitudes of Eqs. (7) and (10) is then given by

$$\begin{aligned}
\sigma_0(K^{\pm}p \to K^{*+}p) &= \tfrac{1}{4}\sigma_0(K^-p \to \overline{K}^{*0}n) \\
&= \langle \sin^2\delta_P \rangle |P^f_0|^2 + \tfrac{1}{3}|S^f_0|^2 \ , \\
\tfrac{1}{4}\sigma_+(K^-p \to \overline{K}^{*0}n) &= \langle \sin^2\delta_P \rangle [\,|P^f_+|^2 + |P^n_+({\rm CEX})|^2\,] \\
&\quad + \tfrac{1}{3}|S^f_0|^2 \ , \\
\sigma_+(K^{\pm}p \to K^{*\pm}p) &= \langle \sin^2\delta_P \rangle [\,|P^f_+|^2 + |P^n_+({\rm NCEX})|^2\,] \\
&\quad + \tfrac{1}{3}|S^f_0|^2 \ ,
\end{aligned} \tag{13}$$

where $\langle \sin^2\delta_P \rangle$ accounts for the rapid $M_{K\pi}$ dependence of the P-wave $K\pi$ phase shift across the mass interval.

B. Results

The isovector parameters of the preceding subsection were determined by performing least-squares fits to the six unnormalized moments of the $K\pi$ angular distributions for reaction (3) in the t range $0 < -t < 0.4$ GeV^2. For $-t < 0.4$ GeV^2, only the q_+ data points were included in the fit. The values of the parameters are listed in Table III, and the fits are shown by the curves on Fig. 6, where they can be seen to provide an excellent description of the t dependence of the charge-exchange reaction.

The parameters describing the isoscalar exchanges were determined from least-squares fits to the data for reactions (1) and (2) with the isovector-exchange parameters determined from the fits to the charge-exchange reaction (3). Both models A and B were found to provide excellent descriptions of the t dependence of both reactions. As an example the fit for model A is shown in Fig. 6. In their description of the 13 GeV/c $K^{*\pm}$ production data the two models are essentially indistinguishable. Although one might have expected the effective f contribution of model B to be the same as the P plus EXD f of model A, with the same ω contributions in each model, this is in fact not the case. In Fig. 7 we show, for three different t values, the isoscalar contributions to P^n_+ for K^{*+} production. From Fig. 7 it is apparent that the ω contribution of model A is much

TABLE III. (a) The parameters describing $\overline{K}^{*0}(890)$ production and the $I_t = 1$ contributions to charged-K^* production at 13 GeV/c. (b) The parameters describing the $I_t = 0$ contributions to charged-K^* production at 13 GeV/c.

(a)

Parameter	Value	Ref. 13	Parameter	Value
$G_{\pi B}$	2.29 ± 0.04	(3.0)	G_c	−3.15 ± 0.12
b_π	2.6 ± 0.1	(2.8)	b_c	4.2 ± 0.3
G_A	20.8 ± 0.5	(20)	γ_s	0.45 ± 0.04
b_A	3.12 ± 0.05	(2.8)	Δ_s	54° ± 4°
			b_s	0.3 ± 0.6

(b)

Model A			Model B	
Parameter	Value	Ref. 13	Parameter	Value
$G^{\rm EXD}_{f\omega}$	58 ± 1	(33)	G_f	59 ± 2
$b_{f\omega}$	3.82 ± 0.07	(2.8)	b_f	4.50 ± 0.08
α'_E	1.12 ± 0.01	(0.9)	G_ω	15 ± 2
G_P	14 ± 3	(9)	b_ω	2.4 ± 0.4
b_P	3.3 ± 0.6	(3)	α'_ω	1.11 ± 0.02

larger than that of model B.

We note that our model A is very similar to that of Irving,[13] who uses a model of strongly EXD Regge poles with SU(3)-symmetric couplings to describe charge-exchange reactions of the type

$$M+B \to M'+B' ,$$

where M, M' (B, B') represent any meson (baryon). Irving calculates the Pomeron by its f, f' coupling, with an overall strength determined from meson resonance production cross sections. In Table III, we compare our parameter values with the corresponding ones calculated from Ref. 13. With the exception of $G_{f\omega}$, there is remarkably good agreement between the two different sets of values. On the other hand, if one believes in the Gribov-Morrison[14] rule or in exact SU(3) for couplings, then the Pomeron cannot couple to the $KK^*(890)$ system. Nonetheless, one might expect[11] the f trajectory to be shifted from that of the ω by f-P mixing. If the energy scale, s_0, is 1 GeV^2, then f-ω couplings which are equal at 1 GeV will lead, via the Regge $(s/s_0)^\alpha$ factor, to a ratio $G_f/G_\omega = 3.7$ at 13 GeV/c, as compared with the value of 4.0 found in the fits of our model B. Thus, at this stage, there is no firm reason for preferring either of our models over the other.

V. MODEL PREDICTIONS FOR OTHER REACTIONS

We have seen that both models A and B provide excellent descriptions of the 13 GeV/c $K^*(890)$ production data. Also, the parameters of both models were found to be in good agreement with expected values. However, these models correspond to very different ω-exchange contributions and also to different trajectories for the dominant isoscalar exchanges. In this section, we take advantage of these differences to compare the predictions of the two models with existing data for (a) the energy dependence of $K^{*\pm}(890)$ production, (b) the cross sections for $K^{*\pm}(1420)$ productions, and (c) the $I_t = 0$ contribution to $\rho^\pm$ production.

A. $K^{*\pm}(890)$ energy dependence

The phase energy relation implies that to calculate an amplitude for K^* production for a beam momentum, P_L, different from 13 GeV/c, the Regge couplings G_R of Eqs. (7) and (10) should be replaced by

$$G_R \to \frac{13}{P_L} G_R \left(\frac{s}{s_{13}}\right)^{\alpha_R(t)} \qquad (14)$$

From the values of the trajectories found in the preceding section, it is clear that model A predicts an asymptotically energy-independent differential cross section at fixed t, whereas model B leads to a $d\sigma/dt$ decreasing like $P_L^{-0.3}$ at small t. From the relative sizes of the various couplings, we expect the onset of the $P_L^{-0.3}$ behavior of model B by about 5 GeV/c, while for model A the asymptotic region, that is, the realm of Pomeron dominance, is not reached until about 300 GeV/c. Another difference between the two models lies in their different predictions for the energy dependence of the ratio

$$R(t) = \frac{(d\sigma/dt)(K^- p \to K^{*-} p) - (d\sigma/dt)(K^+ p \to K^{*+} p)}{\frac{1}{2}[(d\sigma/dt)(K^- p \to K^{*-} p) + (d\sigma/dt)(K^+ p \to K^{*+} p)]} . \qquad (15)$$

In model A, since the size of the Pomeron contribution, relative to the dominant EXD f-ω contribution, is an increasing function of energy, the ratio R increases with energy to a maximum of about 0.44 at $t = 0.1$ GeV^2 at $P_L \simeq 100$ GeV/c and then slowly decreases. In model B, on the other hand, the ω contribution decreases more rapidly than does the dominant f contribution as the energy increases, so that R is a decreasing function of energy. This behavior is illustrated in Fig. 8, where the solid (dashed) line represents the prediction of model A (B) for the energy dependence of $R(t = -0.1)$. For comparison, we have also plotted in Fig. 8 our 13-GeV/c experimental value

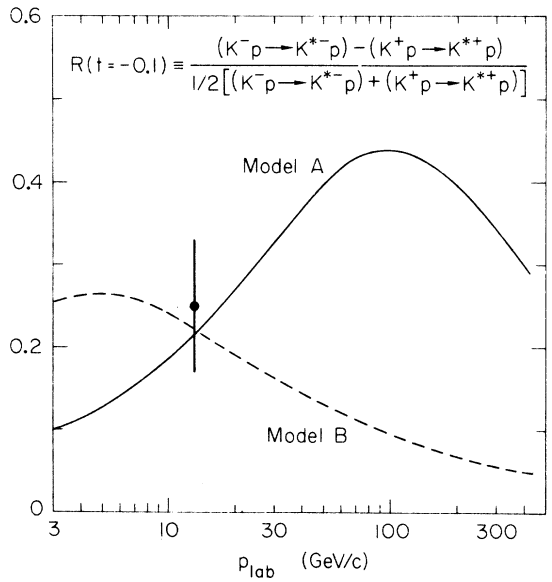

FIG. 8. The predictions of models A (solid line) and B (dashed line), with the 13-GeV/c parameters of Table III, for the energy dependence of the ratio [$R(t)$ of Eq. (15)] of the difference between the K^{*-} and K^{*+} differential cross sections to their average value, at $-t = 0.1$ GeV^2. The data point shown comes from this experiment.

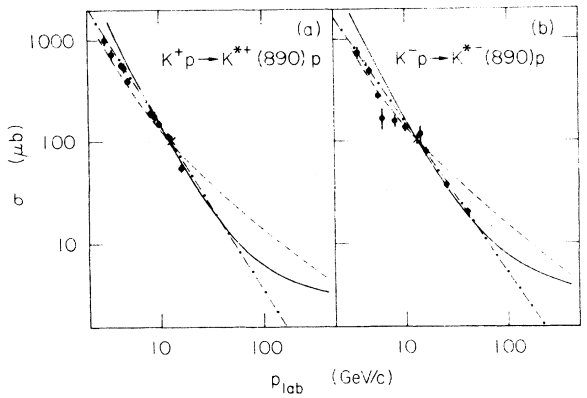

FIG. 9. Comparison of previous data with the predictions obtained using the fit results obtained from model A (solid line) and model B (dashed line) for the energy dependence of $\sigma \equiv \int_{-1}^{0} dt\,(d\sigma/dt)\ [K^{\pm}p \to K^{*\pm}(890)p]$. The dashed-dotted lines represent the p_{lab}^{-n} behavior of Ref. 7. All curves have been constrained to pass through the 13-GeV/c points, represented by an X. Both data and predictions have been corrected to account for the $K^{\pm}\pi^0$ decay modes.

R at $t = 0.1$ GeV^2. Since other $K^{*\pm}$ production experiments have lower statistics (and much larger systematic uncertainties between K^+ and K^- reactions), the uncertainty in the calculation of R at $t = -0.1$ GeV^2 at other energies is about ± 0.2, which is much too large to allow us to distinguish between the two models.

In order to compare the predictions of our two models with $K^{*\pm}$ production data at other energies, it is therefore necessary to compare integrated cross sections. At each of a range of energies from 3 to 400 GeV/c, we use the parametrizations of Eqs. (7) to (13), along with the prescription of Eq. (14), to calculate the cross sections integrated over a $|t|$ range from 0 to 1.0 GeV^2. These predictions, corrected to correspond to a $K^*(890)$ Breit-Wigner form extending from 0.7 to 1.68 GeV and to account for the $K^{\pm}\pi^0$ decay mode of the K^*, are shown in Fig. 9 by the two sets of curves, and in addition are compared with the data of Ref. 7. We emphasize that the curves in Fig. 9 do *not* represent fits to these data points, but are solely an *extrapolation* of our 13-GeV/c results. We see that for $P_L < 8$ GeV/c, model B provides a better description of the energy dependence of $K^{*\pm}$ production, while for P_L between 10 and 40 GeV/c model A is somewhat better. However, since this comparison is obviously very sensitive to the absolute normalization, we feel that it cannot, given the existing experimental data, eliminate either model. In fact, the most definitive means of distinguishing between the two models would be an accurate measurement of the relative K^{*+}, K^{*-} difference, R of Eq. (15) at about 100 GeV/c (see Fig. 8).

B. Predictions for $K^*(1420)$ production

While Regge models specify the energy dependence of K^* production amplitudes, double-Regge models also determine the $M_{K\pi}$ dependence. In these models one calculates the $K^{*\pm}$ production amplitudes at arbitrary $M_{K\pi}$ by making the replacement

$$G_R \to \left(\frac{M_{890}^{\ 2}}{M_{K\pi}^{\ 2}}\right)^{\alpha_R(t)} G_R \tag{16}$$

in Eqs. (7) and (10). Unfortunately, it is not clear whether or not the Pomeron should be treated in this way, particularly since there is no SU(3) restriction on its coupling to $K^*(1420)$ production as there is for $K^*(890)$ production. Nonetheless, we show in Table IV a comparison of the data and of our predictions for $K^*(1420)$ production. We see that model B gives predictions which are in good agreement with the data. However, since it is not clear that such naive Regge prescriptions are quantitatively correct at such low $M_{K\pi}$ values, we are unable to reject model A on the basis of this comparison alone.

C. Predictions for ρ production

SU(3) relates the ω-exchange contribution to $K^*(890)$ production to that for $\rho^{\pm}$ production. From Fig. 7 it is apparent that our two models will provide drastically different predictions for the size of the isoscalar exchange in ρ production. In Fig. 10 we compare the model predictions with the 6- and 16-GeV/c data.[5] We see that, for $-t$

TABLE IV. Predicted and measured values of the cross sections for $K^*(1420)$ production, integrated over $|t|$ from 0 to 0.6 GeV^2. The $K^*(1420)$ is defined by $1.36 < M_{K\pi} < 1.48$ GeV, and the cross sections correspond to the $K^0\pi^{\pm}$ decay mode, assuming, where necessary, $K^*(1420)$ branching fractions $x_{K\pi} = 0.55$ and $x_{K^*\pi} = 0.3$.

	$\sigma(K^{\pm}p \to K^*(1420)^{\pm}p)$ (μb)	
	K^+	K^-
Model A prediction	49	51
Model B prediction	27	30
This experiment, $K^0\pi^{\pm}$decay	24 ± 3	20 ± 3
This experiment, $K^*\pi$ decay	27 ± 3	23 ± 3
10 GeV/c, hydrogen bubble chamber (HBC)[a]		32 ± 5
12 GeV/c, HBC[b]	30 ± 3	
14.3 GeV/c, HBC[c]		26 ± 5
16 GeV/c, HBC[b]	23 ± 3	

[a] M. Deutschmann *et al.*, Nucl. Phys. B36, 373 (1972).
[b] J. N. Carney *et al.*, Nucl. Phys. B107, 381 (1976).
[c] B. Chaurand *et al.*, Phys. Lett. 38B, 253 (1972).

< 0.2 GeV^2, model A is in good qualitative agreement with the data at both energies, while the predictions of model B are only about a tenth as large as the measured cross sections. Both models predict a zero at smaller $-t$ than the data, and both predict higher secondary maxima than the data. In Fig. 11 we compare the $I_t = 0$ contributions to the natural-parity ρ production cross sections[5, 15] with the ratio R of Eq. (15) for K^* production. It is evident that the zeros in these two sets of data are consistent with being at the same t value. We therefore conclude that model A provides a good qualitative description of the ρ production data while the description of model B is definitely unacceptable.

D. General properties of the $I_t = 0$ exchange amplitude

It is possible, from the above comparisons of our model predictions with previous data, to infer the properties which must be possessed by any model describing not only the 13-GeV/c $K^*(890)$ production but also the quantitative features of (a) the energy dependence of the $K^*(890)$ cross section, (b) $K^*(1420)$ production, and (c) $\rho^\pm$ production. In the first place, both the energy dependence below 10 GeV/c and $K^*(1420)$ production require that the trajectory of the dominant isoscalar exchange have a value of about 0.6 at small $-t$. The location of the zero in the isoscalar contribution to $\rho^\pm$ production, in conjunction with the positions of the K^+/K^- crossover in $K^{*\pm}$ production, requires that the ω trajectory have a zero at $-t \sim 0.4$ GeV^2. The magnitude of $\rho^\pm$ production via $I_t = 0$ exchange implies that the size of the ω contribution to the $I_t = 0$ K^* production cross section must be about one-third that of the dominant f (or $f + P$) contribution. It should be possible to satisfy these criteria in the context of either of the two models presented here.

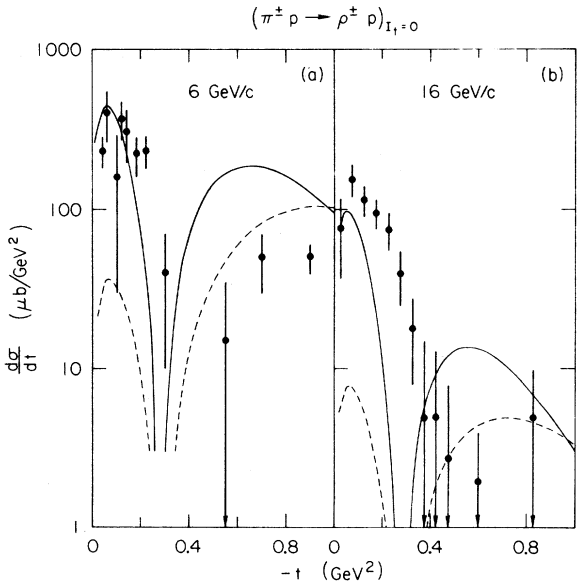

FIG. 10. Comparison of the data with the predictions of models A (solid line) and B (dashed line) using the 13-GeV/c parameters of Table III, for the isoscalar-exchange contributions to $\rho^\pm$ production at 6 and 16 GeV/c, Ref. 5.

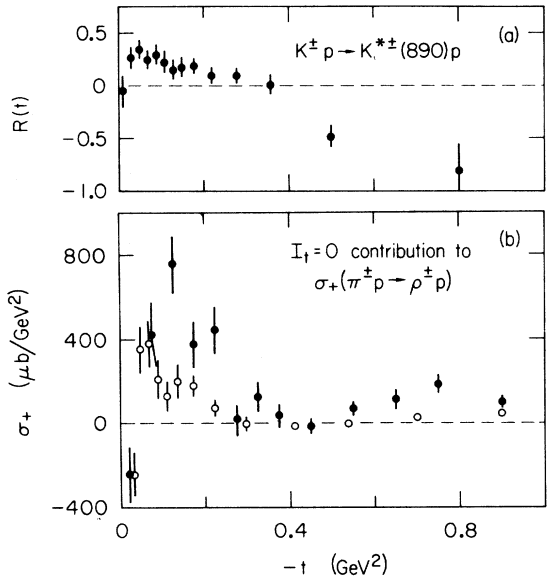

FIG. 11. (a) The t dependence of the ratio $R(t)$ of Eq. (15) for $K^*(890)$ production at 13 GeV/c. (b) The t dependence of the isoscalar-exchange contribution to $\sigma_+(\pi^\pm p \to \rho^\pm p)$ at 3.9 GeV/c (solid points) and 6.0 GeV/c (open circles).

VI. CONCLUSIONS

We have presented high-statistics data on differential cross sections and density matrix elements for $K^{*\pm}(890)$ production at 13 GeV/c with good K^+/K^- relative normalization. These data show that $K^{*\pm}(890)$ production is dominated by natural-parity isoscalar exchange and that there are significant differences between the K^{*+} and K^{*-} reactions. We have proposed two models, differing only in their parametrization of the natural-parity isoscalar exchanges, to describe the data: (A) a model involving a Pomeron and strongly exchange-degenerate ω-f Regge poles and (B) a model with no Pomeron and ω-f exchange degeneracy broken. Both models were found to provide good descriptions of the t dependence of the data at 13 GeV/c and to give reasonable values for couplings and slope parameters. We have also presented the predictions of both models for 13-GeV/c $K^*(1420)$

production, for the energy dependence of $K^*(890)$ production, and for the isoscalar-exchange contribution to ρ production at 6 and 16 GeV/c. On the basis of these comparisons, we conclude that (i) for the dominant $I_t = 0$ exchange, $\alpha \sim 0.6$ at small $-t$, (ii) $\alpha_\omega(t \sim -0.4) = 0$, and (iii) that ω exchange makes a significant contribution to 13-GeV/c $I_t = 0$ K^* production cross section.

ACKNOWLEDGMENTS

We would like to thank R. Bierce, A. Kilert, D. McShurley, and W. Walsh for their important contributions in the execution of this experiment. This work was supported by the National Research Council of Canada and the U.S. Energy Research and Development Administration.

---

*Present address: Carleton University, Ottawa, Canada.

†Present address: Dept. of Physics, MIT, Cambridge, Mass.

‡Present address: Dept. of Physics, Oxford University, Oxford, England.

§Present address: Ecole Normale Superieure, Laboratoire de l'Accelerateur Lineaire, F-91, Orsay, France.

¶Present address: Dept. of Physics, Johns Hopkins Univ., Baltimore, Md.

||Present address: TRIUMF, Univ. of British Columbia, Vancouver, B. C., Canada.

[1]P. Estabrooks and A. D. Martin, Nucl. Phys. B102, 537 (1976).

[2]P. Estabrooks *et al.*, Phys. Lett. 60B, 473 (1976).

[3]A. B. Wicklund *et al.*, Phys. Rev. D 17, xxx (1978); in *Proceedings of the XVII International Conference on High Energy Physics, London, 1974,* edited by J. R. Smith (Rutherford Laboratory, Chilton, Didcot, Berkshire, England, 1974).

[4]G. W. Brandenburg *et al.*, Phys. Lett. 59B, 405 (1975).

[5]D. Crennell *et al.*, Phys. Rev. Lett. 27, 1674 (1971); B. Haber *et al.*, Phys. Rev. D 10, 1387 (1974); J. Bartsch *et al.*, Nucl. Phys. B46, 46 (1972).

[6]C. Michael, Nucl. Phys. B57, 292 (1973).

[7]J. N. Carney *et al.*, Nucl. Phys. B107, 381 (1976); M. Deutschmann *et al.*, *ibid.* B81, 1 (1974).

[8]M. M. Nagels *et al.*, Nucl. Phys. B109, 1 (1976).

[9]The quantitative results and structure of this exchange amplitude will be developed in Sec. IV.

[10]A. V. Barnes *et al.*, Phys. Rev. Lett. 37, 76 (1976); O. I. Dahl *et al.*, *ibid.* 37, 80 (1976).

[11]P. R. Stevens, G. F. Chew, and C. Rosenzweig, Nucl. Phys. B110, 355 (1976).

[12]Note that this sign is an agreement with simple EXD (duality) expectations.

[13]A. C. Irving, Nucl. Phys. B121, 176 (1977).

[14]V. N. Gribov, Yad. Fiz. 5, 197 (1967) [Sov. J. Nucl. Phys. 5, 138 (1967)]; D. R. O. Morrison, Phys. Rev. 165, 1699 (1968).

[15]Note that the (small) differences between the $I_t = 0$ ρ production cross sections of Fig. 10 and the σ_+ of Fig. 11 must be due to unnatural-parity isoscalar exchange which we have completely neglected in our models.